QUARTERLY JOURNAL OF THE ROYAL METEOROLOGICAL SOCIETY
Q. J. R. Meteorol. Soc. **134**: 889–904 (2008)
Published online 23 May 2008 in Wiley InterScience
(www.interscience.wiley.com) DOI: 10.1002/qj.252

Cloud-resolving ensemble simulations of the August 2005 Alpine flood

Cathy Hohenegger,[a]* André Walser,[b] Wolfgang Langhans[c] and Christoph Schär[a]
[a] *Institute for Atmospheric and Climate Science, ETH Zürich, Switzerland*
[b] *Federal Office of Meteorology and Climatology, MeteoSwiss, Zürich, Switzerland*
[c] *Institute of Meteorology and Geophysics, University of Innsbruck, Austria*

ABSTRACT: In this study we explore the potential benefits of applying a cloud-resolving ensemble prediction system (EPS; 2.2 km grid spacing) over its driving synoptic-scale limited-area EPS (COSMO-LEPS, 10 km grid spacing, driven by the ECMWF EPS) for a case of heavy precipitation over the Alpine region. The selected event is the devastating August 2005 flood that affected the northern Alpine slopes. The cloud-resolving EPS includes an explicit treatment of deep convection and dynamically downscales the COSMO-LEPS information. Results are compared against rain-gauge and radar data. Furthermore, the sensitivity of the results to initial versus lateral boundary uncertainties are analyzed using a series of additional simulations.

Comparison of the cloud-resolving and its driving limited-area EPS pinpoints the high skill of both ensembles in simulating the major phase of heavy precipitation. The high-resolution EPS yields more realistic rain amounts, in particular in areas of active convection, but in general the resolution-induced differences tend to be smaller than typical member-to-member variability. The differences between the two ensembles can be tied to the synoptic situation (stratiform or convective precipitation, location of the cyclone), to the mesoscale interaction of the flow with the topography (flow over the Alpine ridge), and to the experimental set-up (lead time and computational domain).

For the considered event and set-up, the growth of initial perturbations dominates over lateral boundary uncertainties during the first ∼12 integration hours. Afterwards, the ensemble spread is controlled by large-scale error growth advected from the lateral boundaries into the domain. Copyright © 2008 Royal Meteorological Society

KEY WORDS ensemble prediction; quantitative precipitation forecasting; high-resolution NWP; severe weather

Received 12 September 2007; Revised 3 March 2008; Accepted 28 March 2008

1. Introduction

Heavy precipitation frequently occurs over the Alpine region due to the proximity of the Atlantic and the Mediterranean Sea, and due to the important role of orographic effects (e.g Schär *et al*., 1998; Buzzi *et al*., 1998; Smith, 1979). The Alpine flood of 19–24 August 2005 was a particularly strong event and hit Switzerland, Austria and Germany (MeteoSchweiz, 2006; Zängl, 2007a,b; Jaun *et al*., 2008). The same event also affected Romania. In total, 49 people were killed. The economical costs have been estimated at 1.86 billion US$ insured losses and 3.3 billion US$ total damage (SwissRe, 2006). On a global perspective, this places the event as the fifth most costly insurance loss of the year 2005, after the Atlantic hurricanes *Katrina*, *Rita*, *Wilma*, and the European winter storm *Erwin*. The August 2005 flood is also classified as the worst flood in Europe since 2002. In Switzerland, record-breaking values of precipitation were observed. In Central Switzerland, 5-day precipitation totals exceeded 200–300 mm, corresponding to return periods greater than 150 years (MeteoSchweiz, 2006; Bezzola and Hegg, 2007). As a result, record discharge and lake levels were registered at many stations. As an example, the level of Lake Sarnen (46°52′N, 8°13′E, area 7.5 km^2, maximum depth 51 m) exceeded the previous high-water mark by as much as 1.20 m. Water and landslides severely affected buildings, roads, and railway transportation. The river Aare entered the old town of Berne, causing a damage of 40 million US$. In mountain areas, numerous villages were cut off. The reopening of some railway lines (e.g. the connection to Engelberg) was not achieved until December 2005. Similar damage has been documented for Austria, especially in the Voralberg and Tyrol regions (Kanonier, 2006; BMLFUW, 2006), and in southern Germany (LFU, 2006; Rudolf *et al*., 2006). Triggered by the staggering event, governmental action is being taken in several Alpine countries to help mitigate the consequences of future events by improved flood protection measures as well as refined warning and response procedures (MeteoSchweiz, 2006; Bezzola and Hegg, 2007).

The development of accurate medium- to short-range prediction systems and adequate response strategies appear especially important since heavy precipitation events over northern and central Europe have shown an

* Correspondence to: Cathy Hohenegger, Institute for Atmospheric and Climate Science, ETH Zürich, Universitätstr. 16, 8092 Zürich, Switzerland. E-mail: cathy.hohenegger@env.ethz.ch

increasing trend over the last century (e.g. Klein Tank and Können, 2003; Schmidli and Frei, 2005). For the next century, regional climate change scenarios that account for increasing greenhouse gas concentrations suggest a further increase in the frequency of extreme events to the north of the Alps (e.g. Christensen and Christensen, 2003; Frei *et al*., 2006).

Unfortunately, the skill of quantitative precipitation forecasting (QPF) is still rather poor (e.g. Ebert *et al*., 2003; Kaufmann *et al*., 2003). The application of limited-area ensemble prediction systems (LEPS) with grid spacings of $\mathcal{O}$(10 km) has provided added value for QPF purposes (e.g. Grimit and Mass, 2002; Montani *et al*., 2003; Marsigli *et al*., 2004, 2005; Eckel and Mass, 2005; Yuan *et al*., 2005). A LEPS integrates a set of simulations generated by perturbing the model initial state, the lateral boundary conditions, and/or the physical parametrizations. As an example, the operational COSMO-LEPS suite employs representative members selected from the European Centre for Medium-Range Weather Forecasts (ECMWF) global EPS as initial and lateral boundary conditions, and uses randomly chosen convective parametrizations for the integration of the high-resolution forecast (Marsigli *et al*., 2005).

The emergence of cloud-resolving models with grid spacings of $\mathcal{O}$(1 km) has opened further prospects to improve the skill of QPF (Brooks *et al*., 1992; Benoit *et al*., 2002; Fritsch and Carbone, 2004). The higher resolution allows a better representation of the topography and of the surface fields, and an explicit treatment of moist convection (or parts of it). Several studies have assessed the benefits of cloud-resolving model mesh sizes (e.g., Mass *et al*., 2002; Richard *et al*., 2003a; Buzzi *et al*., 2004; Colle *et al*., 2005; Richard *et al*., 2007; Zängl, 2007b). It is generally accepted that such integrations yield more realistic precipitation patterns and are more skilful in cases of moist convection and/or over regions of complex topography. However, the achieved gain is often not significant in terms of statistical skill scores (Mass *et al*., 2002).

Owing to the limited atmospheric predictability and motivated by the success of LEPS (see above references), cloud-resolving simulations may be most promising in an ensemble mode, as first postulated by Brooks *et al*., (1992). So far, however, only relatively little experimentation is available. Some studies (e.g. Zhang *et al*., 2003; Walser *et al*., 2004; Hohenegger *et al*., 2006) have conducted cloud-resolving ensemble simulations with perturbed initial conditions to investigate aspects of the mesoscale predictability of selected weather events. Kong *et al*., (2006, 2007) have explored a full cloud-resolving EPS approach. They generated a 3 km ensemble that employed different initial and lateral boundary conditions, and examined its performance for a tornadic thunderstorm event. They concluded that the 3 km ensemble outperformed its coarser-resolution counterpart. In their case, certain ensemble members were able to capture storm-scale features that were absent in the control (deterministic) forecast.

Even beyond the excessive computational costs, short-range cloud-resolving ensemble prediction systems pose a number of challenges. As compared to traditional synoptic-scale EPS, the use of smaller integration domains and of non-hydrostatic models allows for very rapid error propagation (Hohenegger and Schär 2007a). Small-scale initial uncertainties are able to contaminate the full integration domain in a few hours and, depending upon the overall synoptic situation, to effectively limit predictability. In comparison to traditional EPS, cloud-resolving error doubling times, which primarily relate to convective rather than baroclinic instability, are an order of magnitude larger (e.g. Zhang *et al*., 2003; Hohenegger and Schär 2007b). Cloud-resolving simulations also show tremendous nonlinearities, and the tangent-linear approximation fails after some few hours. In terms of tangent-linear approximation, a 10-day synoptic-scale forecast is comparable to merely a 7-hour cloud-resolving integration (Hohenegger and Schär 2007b). Further difficulties arise due to the nesting of multiple grids (e.g. Nutter *et al*., 2004; Kong *et al*., 2007). As a consequence, many traditional ensemble strategies (e.g. singular vectors, breeding modes; Kalnay, 2003), which are common practice in synoptic-scale forecasting, are largely uncharted territory in cloud-resolving applications.

In this study, we seek to assess the potential benefits of using a cloud-resolving EPS over its driving lower-resolution LEPS for a case of heavy precipitation over the Alpine region. Since the design of an optimal ensemble is an open question at such scales, we will also investigate the sensitivity of the cloud-resolving simulations to the chosen initial perturbations and the contribution of initial versus lateral boundary uncertainties to the generated spread.

In order to pursue our goals, we apply a high-resolution (2.2 km) numerical weather prediction (NWP) model integrated in an ensemble mode. The considered event is the August 2005 Alpine flood. The ensemble includes perturbed initial and lateral boundary conditions but neglects the modelling error term (e.g. no stochastic physics). The computational domain and some of the dynamical and physical packages are similar to the ones employed in previous predictability studies (Hohenegger *et al*., 2006; Hohenegger and Schär, 2007a,b), but in contrast to these former studies we also account for uncertainties stemming from the lateral boundary conditions.

Our study has two main restrictions. First, we neglect the modelling error term. As shown by several sensitivity studies (e.g. Richard *et al*., 2003b; Zängl, 2004b), this component can have a significant impact on the simulated flow and should be incorporated in an operational set-up. Second, we focus on one single case of heavy precipitation. One event is obviously not sufficient to provide reliable statistical validation. Our study may thus be viewed as a pilot study highlighting the possible strengths and weaknesses of a cloud-resolving EPS compared to its driving LEPS.

DOI: 10.1002/qj

The outline is as follows. Section 2 presents in more details our methodology with a description of the model, the set-up of the ensemble experiments, and the observational data. Section 3 describes the synoptic situation of the simulated Alpine flood event. Section 4 compares the cloud-resolving EPS and its driving LEPS and interprets the observed resolution-induced differences. The second part of the results, the sensitivity of the cloud-resolving simulations to the specification of initial and lateral boundary perturbations, follows in Section 5. Conclusions are given in Section 6.

2. Methods

2.1. The COSMO model

The model of the consortium for small-scale modelling (COSMO), formerly known as Lokal Modell (LM), is a non-hydrostatic limited-area model developed for operational purposes (Steppeler *et al*., 2003). Its physical and dynamical packages have recently been updated for cloud-resolving applications (Doms and Förstner 2004). The COSMO model is based on the unfiltered fully compressible primitive equations integrated by the time-splitting technique (Klemp and Wilhelmson, 1978; Skamarock and Klemp, 1992) and a second-order leapfrog HE-VI (horizontally explicit-vertically implicit) scheme. Precipitation processes include prognostic rain, snow, and ice (Baldauf and Schulz, 2004). Recent sensitivity studies (e.g. Verbunt *et al*., 2007) have shown the importance of the horizontal advection of hydrometeors over complex topography at the resolutions considered. For cloud-resolving applications, deep convection is explicitly resolved while shallow convection is parametrized after Tiedtke (1989). At coarser grid spacing, the Tiedtke mass flux scheme is used. Computation of the turbulent vertical transport of moment and heat employs a closure at level 2.5 (in the notation of Mellor and Yamada, 1982) and is based on turbulent kinetic energy considerations (Raschendorfer, 2001). Further physical packages comprise a multi-layer soil model (Heise *et al*., 2003) and the Ritter and Geleyn (1992) radiative transfer scheme. The boundary conditions are updated in a one-way-nesting strategy and relaxed after Davies (1976), where the associated weights fall below 0.01 after six grid points.

2.2. Limited-area EPS: COSMO-LEPS

COSMO-LEPS is an operational limited-area EPS designed for the prediction of intense and localized weather events in the short to medium range. In its operational application, it employs a clustering technique (Molteni *et al*., 2001) to select representative members from the two most recent global ECMWF ensemble forecasts (102 members). They provide the initial and lateral boundary conditions for limited-area simulations with COSMO (Marsigli *et al*., 2001). For our study, we use the COSMO-LEPS configuration with 10 representative members (selected from one 51-member ECMWF ensemble). For each of them, the COSMO model (version 3.16) is integrated on a rotated spherical grid with a mesh size of 0.09° (10 km) and 32 vertical levels over a domain covering central and southern Europe (Figure 1(a)). Simulations start at 12 UTC on 20 August 2005. This ensemble is referred to as COSMO10 (Table I). While COSMO10 assumes a perfect model, the driving global EPS also accounts for model uncertainties by applying stochastic physics (Buizza *et al*., 1999). The driving ECMWF EPS uses dry singular vectors as initial perturbations (e.g. Molteni *et al*., 1996; Buizza *et al*., 2005).

In addition to COSMO10, a control simulation named CTL10 is integrated. Its initial and lateral boundary conditions are derived from the ECMWF EPS control run.

2.3. Cloud-resolving EPS

The cloud-resolving EPS is integrated over the Alpine region (Figure 1(b)) with COSMO (version 3.16) at a

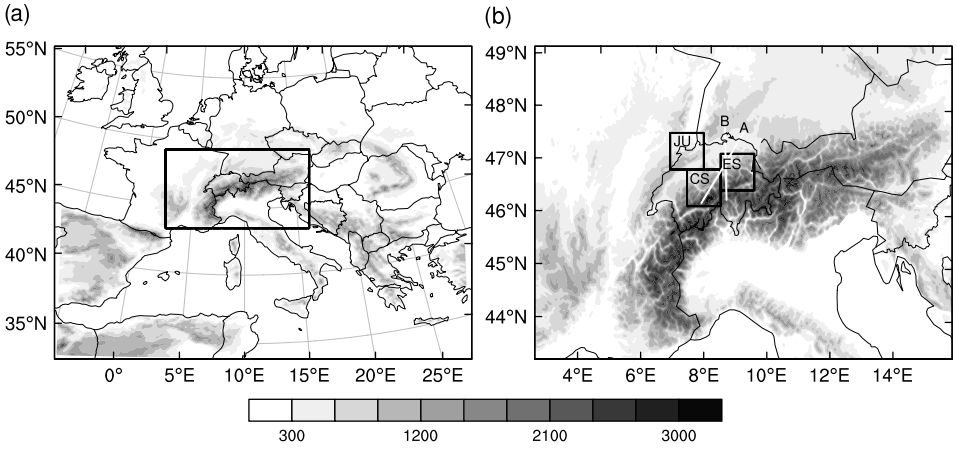

Figure 1. Integration domain and topography (m) of the (a) 10 km and (b) 2.2 km COSMO simulations. Locations of the two cross-sections used to construct Figure 4 and of the three subdomains JU (Jura), CS (central Switzerland), and ES (eastern Switzerland) used in Figures 8 and 11 are indicated. The subdomains each cover an area of circa 90 km × 79 km.

DOI: 10.1002/qj

Table I. Characteristics of the different simulations and ensembles.

Name	Mesh size	Topography	Deep convection	Members	Initial conditions	Lateral boundaries
CTL10	0.09°	10 km	Tiedtke	1	ECMWF EPS control run	ECMWF EPS control run
COSMO10	0.09°	10 km	Tiedtke	10	ECMWF EPS SV	ECMWF EPS
COSMO2.2	0.02°	2.2 km	explicit	10	COSMO10 downscaled SV	COSMO10
COSMO2.2T10	0.02°	∼10 km	explicit	10	COSMO10 downscaled SV	COSMO10
COSMO2.2INI	0.02°	2.2 km	explicit	10	COSMO10 downscaled SV	CTL10 identical
COSMO2.2INIsub	0.02°	2.2 km	explicit	4	COSMO10 downscaled SV	CTL10 identical
SHIFT2.2	0.02°	2.2 km	explicit	4	CTL10 shifted initialization	CTL10 identical

Mesh size 0.09° = 10 km; 0.02° = 2.2 km.
SV = singular vectors.

horizontal resolution of 0.02° (2.2 km) and with a large time step of 12 s. The computational domain contains 501 × 301 grid points in the horizontal and 45 hybrid vertical levels.

The first ensemble, denoted COSMO2.2 (Table I), utilizes as initial and lateral boundary conditions the ten COSMO10 members. Simulations start at 1200 UTC on 20 August 2005 and are integrated for a period of 72 hours to cover the phase of heavy precipitation occurring over central Switzerland. The major differences between COSMO2.2 and COSMO10 concern their respective grid spacing, the resolution of the external parameter fields (especially topography), and the treatment of moist convection (Sections 2.1 and 2.2). To isolate the role of fine-scale topography, a slightly modified version of COSMO2.2, named COSMO2.2T10, is also considered. As sole difference to COSMO2.2, COSMO2.2T10 utilizes a filtered representation of the COSMO2.2 topography, shaped to resemble the COSMO10 version (Table I).

The choice of the members' initial and lateral boundary conditions is a critical factor for the generation of a well-behaved ensemble, but is still a largely unresolved issue for limited-area integrations. The sampling strategy of the cloud-resolving simulations follows COSMO10. In this respect, the constructed perturbations may not be optimal. In particular, the downscaled ECMWF singular vectors are designed for synoptic-scale applications. They do not include any mesogamma-scale features at initial time, which are known to affect high-resolution simulations (e.g. Ducrocq *et al*., 2002; Richard *et al*., 2007).

To investigate the sensitivity of the 2.2 km integrations to the representation of initial and lateral boundary uncertainties, three further ensembles denoted COSMO2.2INI, COSMO2.2INIsub, and SHIFT2.2 are constructed (Table I). COSMO2.2INI starts from the downscaled singular vectors (as COSMO2.2) but uses identical lateral boundary conditions for each member. The lateral boundary conditions stem from CTL10. Comparison of COSMO2.2INI and COSMO2.2 allows isolating the contribution of the initial uncertainties to the total spread.

The last two ensembles, COSMO2.2INIsub and SHIFT2.2, have been constructed to test the role of the chosen initial perturbations within ensembles that utilize identical lateral boundary conditions. COSMO2.2INIsub contains a subset of COSMO2.2INI made of four integrations. Those correspond to members 2, 5, 3, and 8, the representative members of the four most populated clusters. COSMO2.2INIsub thus employs downscaled singular vectors as initial perturbations. In contrast, SHIFT2.2 uses a shifting initialization technique (Walser *et al*., 2004, their Figure 2). The first member is initialized at 1200 UTC on 20 August 2005, with initial and lateral boundary conditions derived from CTL10. The second member starts one hour later, and so on until 1500 UTC for the fourth and last member. All the simulations use CTL10 as lateral boundary conditions. The two ensembles COSMO2.2INIsub and SHIFT2.2 only contain four members to minimize the time delay induced by the shifting initialization technique, during which the COSMO2.2 initial perturbations amplify. Their initial perturbations differ fundamentally since

DOI: 10.1002/qj

they are characterized, respectively, by large-scale (COSMO2.2INIsub) and mesogamma-scale (SHIFT2.2) features.

2.4. Observational data

Observations are derived from the precipitation analysis of MeteoSwiss (MeteoSchweiz, 2006; Frei, 2006). This dataset, referred to as OBSD, contains daily accumulated precipitation records from 482, 842, and 605 rain-gauges located over Switzerland, Austria, and southern Germany, respectively. The data have been interpolated on a grid of ~ 2 km mesh size by utilizing a distance-weighing interpolation scheme and a directional clustering technique as described in Frei and Schär (1998). The effective horizontal resolution amounts to 10–15 km over flat terrain and to 15–20 km over the Alps.

Second, we use the precipitation dataset compiled by Wüest *et al*. (2008, personal communication) to validate simulated hourly precipitation values. The analysis procedure combines the advantages of the radar (high resolution in space and time) and rain-gauge (high accuracy of daily totals at stations) measurements. The disaggregation employs radar sequences to distribute the daily accumulated rain-gauge measurements over each of the 24 hours. The procedure preserves the daily precipitation sums. Due to orographic shadowing of radar observations, the accuracy of this second dataset, named OBSH, is questionable over the Alpine valleys. OBSH is only available over Switzerland.

3. Synoptic-scale situation

Figure 2 illustrates the synoptic situation associated with the August 2005 Alpine flood in terms of the 850 hPa geopotential height field (derived from the ECMWF analysis) at times of heavy rainfalls over Switzerland. The weather evolution (MeteoSchweiz, 2006) was determined by the presence of a low pressure system. This low formed over northern Italy on 20 August and slowly propagated eastward. Its pathway partly followed the track of so-called Vb cyclones (after the classification of Bebber, 1890), which often produce intense precipitation over the northern Alpine slopes (e.g. Keil *et al*., 1999; Zängl, 2004a; Petrow *et al*., 2006). The heavy rain followed from the position of the surface low pressure system advecting warm moist air from the Mediterranean Sea over the eastern Alpine flanks and back towards the northern Alpine slopes. The precipitation then resulted from orographic lifting, and the duration and severity of the event from the quasi-stationarity of the synoptic setting.

For the considered event, widespread precipitation began on 20 August over Switzerland and lasted until the morning of 23 August (MeteoSchweiz, 2006). The most active phase occurred between midday 21 August to the end of 22 August with uninterrupted rainfalls (Figure 5). On 22 and 23 August, intense precipitation also fell over southern Germany and western Austria in agreement with the eastward displacement of the low (e.g. Rudolf *et al*., 2006; BMLFUW, 2006).

Figure 3 shows the 850 hPa geopotential height field of the representative members of the three most populated clusters of COSMO10 for a lead time of 36 hours (i.e. 0000 UTC on 22 August 2005). Comparison with Figure 2(b) illustrates the very good agreement between simulated and analyzed large-scale flow, in the sense that all three members yield a surface low over northern Italy. Note however that the three members place the centre of the low over the Gulf of Genoa (Figure 3(a)), over the Adriatic Sea (Figure 3(b)), and over the Mediterranean Sea along the Italian coast (Figure 3(c)) accompanied by slight shifts in wind direction to the north of the Alps. Such differences are known to affect the associated precipitation distributions.

Besides differences in the large-scale flow, a further characteristic that affects the simulated precipitation is the overall degree of stability and the presence of moist convection. Figure 4 displays cross-sections of the moist Brunt–Väisälä frequency and of the cloud liquid water content at two times of heavy rainfalls over Switzerland. The fields are taken from member 2 of COSMO2.2 (i.e. most populated cluster), but similar results are obtained with most of the other members. The moist Brunt–Väisälä frequency is here chosen as an instability indicator since Fuhrer and Schär (2005) have shown

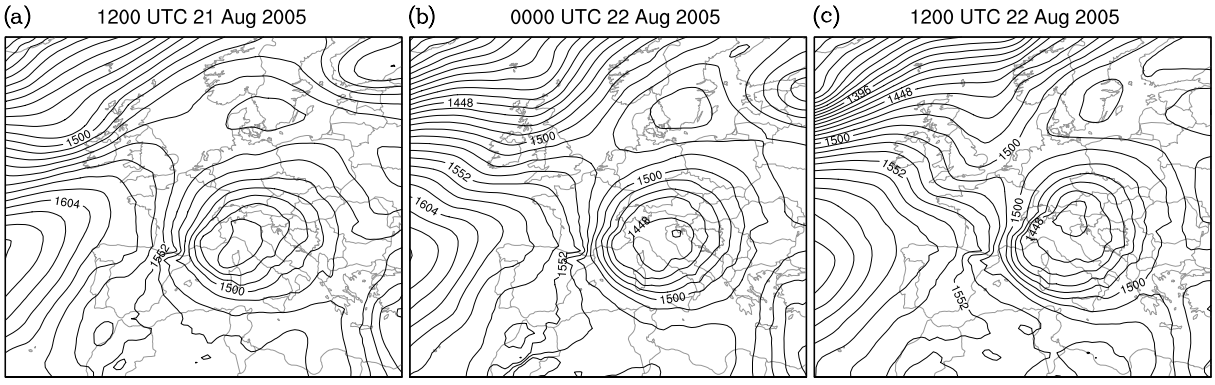

Figure 2. 850 hPa geopotential height fields (m) from the ECMWF analysis valid at (a) 1200 UTC on 21 August, (b) 0000 UTC on 22 August, and (c) 1200 UTC on 22 August 2005.

DOI: 10.1002/qj

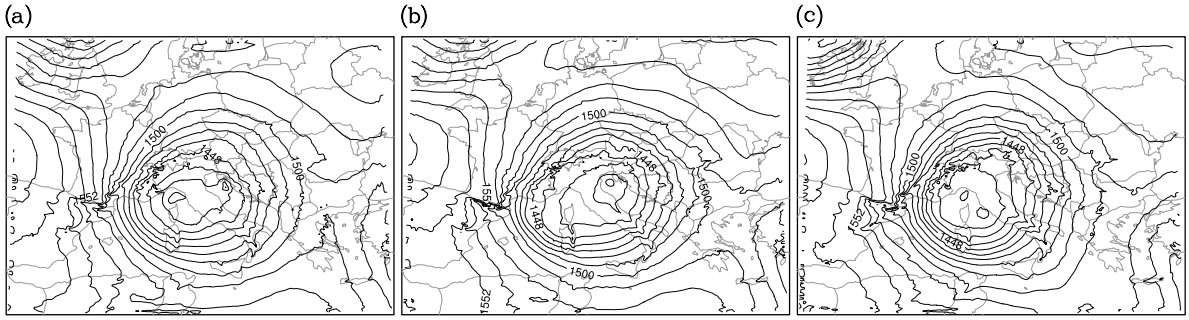

Figure 3. 850 hPa geopotential height (m) obtained from 36-hour forecasts valid at 0000 UTC on 22 August 2005 from the representative members of the three most populated clusters of COSMO10: (a) member 2, (b) member 5, and (c) member 3.

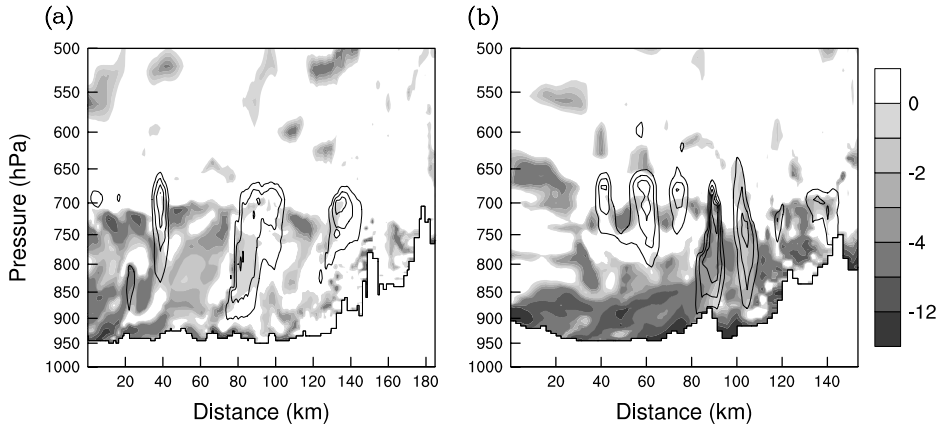

Figure 4. Cross-sections of the moist Brunt–Väisälä frequency (shading, 10^{-5} s^{-2}) and cloud liquid water content (contour interval 0.2 g kg^{-1}) obtained in member 2 of COSMO2.2 at (a) 1900 UTC on 21 August 2005 (cross-section A in Figure 1(b)) and at (b) 1600 UTC on 22 August 2005 (cross-section B in Figure 1(b)).

that it is most skilful at predicting the occurrence of convective cells in idealized simulations of moist flow past topography. Its computation follows Durran and Klemp (1982).

Inspection of Figure 4 reveals that the low-level warm moist air advected by the low towards the Alps is largely unstable. The moist Brunt–Väisälä frequency is predominantly negative below 700 hPa with values up to -12×10^{-5} s^{-2}, while the strength of the equivalent potential temperature inversion amounts to about 9 K (not shown). Also, besides stratiform clouds, shallow cellular cloud structures can be recognized in Figure 4. This pinpoints the presence of embedded shallow convection in the simulated flow.

4. Horizontal resolution and ensemble QPF

This section compares in more detail the performance of the cloud-resolving EPS COSMO2.2 and of its driving lower-resolution EPS COSMO10 in terms of QPF. We focus primarily on the phase of heavy rainfalls occurring between 21 and 22 August 2005 over the northern Alpine slopes (see Section 3).

4.1. Basic results

Figure 5 illustrates ensemble means and observations derived for 20, 21, and 22 August 2005. Note that, although we use the ensemble mean to assess the quality of our ensemble (as in many other studies), it is not obvious in principle that the ensemble mean should fit the observations for an optimal ensemble forecast. Comparison of the precipitation patterns pinpoints the generally high level of agreement between simulations and observations on 21 and 22 August 2005. The phase of heavy rainfalls located over the northern Alpine slopes is well captured both by COSMO2.2 and COSMO10.

A more detailed comparison of the precipitation fields reveals some discrepancies. The 2.2 km ensemble mean exhibits a finer scale and in this sense more realistic structure than its 10 km counterpart. Nevertheless, with the exception of 20 August, the large-scale patterns strongly correlate. On 20 August, COSMO2.2 yields a precipitation maximum over the Jura region instead of the Swiss Plateau compared to OBSD (and to COSMO10), while the two ensembles underestimate precipitation over Austria and southern Germany. This latter effect might be partly related to the fact that the simulations start six hours later than the rain-gauge measurements (see Section 2). On 21 August, COSMO10 overestimates the observed amounts over northeastern Switzerland. COSMO2.2, in contrast, likely underestimates precipitation in central Switzerland. COSMO2.2 and COSMO10 also tend to shift the precipitation band observed over southeastern Germany towards the Austrian boundary. On 22 August, finally, the simulated

DOI: 10.1002/qj

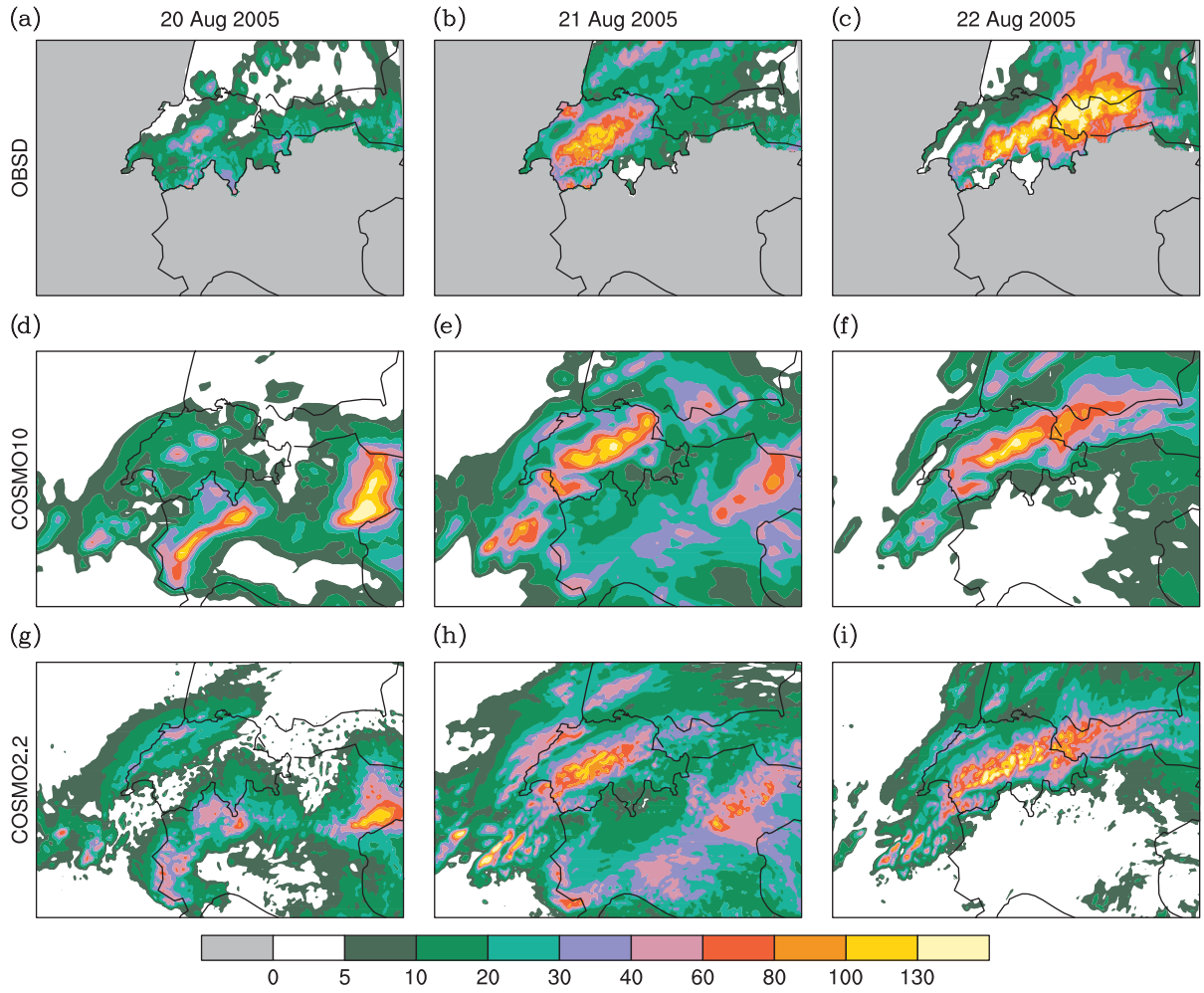

Figure 5. Observations and ensemble means of the accumulated precipitation (mm; from 0600 to 0600 UTC) obtained with (a–c) OBSD, (d–f) COSMO10, and (g–i) COSMO2.2 for (a,d,g) 20 August 2005, (b,e,h) 21 August 2005, and (c,f,i) 22 August 2005. Note that the COSMO10 and COSMO2.2 means lack the first six hours on 20 August (due to simulations beginning at 1200 UTC) and are thus expected to underestimate the observed rainfalls. Note also that the observations are available only over Switzerland, Austria, and southern Germany; grey shading denotes missing data.

rainfall values are too weak over Austria and parts of eastern Switzerland. As a consequence, COSMO2.2 subjectively outperforms COSMO10 on 21 August, while it is less skilful on 20 August. On 22 August, both ensembles perform comparably and COSMO2.2 is unable to correct for an underestimation of precipitation present in COSMO10 over Austria. These visual impressions are confirmed by computing spatial correlation coefficients between observations and simulations, which amount to 0.28 (0.49), 0.79 (0.73), and 0.70 (0.69) for COSMO2.2 (COSMO10) on 20, 21 and 22 August, respectively. Looking at shorter accumulation periods yields a similar picture (not shown).

Concerning the remaining integration domain where no observations are available (Figure 5), the good agreement between the large-scale precipitation pattern of COSMO2.2 and of COSMO10 is generally confirmed. Locally, strong discrepancies in the simulated amounts may appear, as for instance over the western slopes of the Massif Central in France, which receive more than 130 mm in COSMO2.2 versus 30 mm in COSMO10 on 21 August. Also, COSMO2.2 yields notably weaker rainfalls over northern Italy on 20 August.

Figure 6 attempts to assess the significance of the resolution-induced differences by contrasting them with the obtained member-to-member variability (differences between two 10 km integrations) with the help of a Taylor diagram (Taylor, 2001). The 2.2 km results have here been averaged on the 10 km grid. A Taylor diagram compares a pair of integrations (m_1, m_2) on the basis of their spatial correlation r and of the ratio of their spatial standard deviations, $\sigma = \sigma_{m2}/\sigma_{m1}$. The azimuthal location of an entry in the Taylor diagram defines its correlation, while the distance to the origin $(0, 0)$ gives σ. Moreover, the distance to the reference point $(1, 0)$ yields the normalized root-mean-square difference

$$E = \frac{1}{\sigma_{m1}}\left[\frac{1}{N}\sum_{n=1}^{N}\{(m_{1n} - \overline{m_1}) - (m_{2n} - \overline{m_2})\}^2\right]^{1/2}, \quad (1)$$

DOI: 10.1002/qj

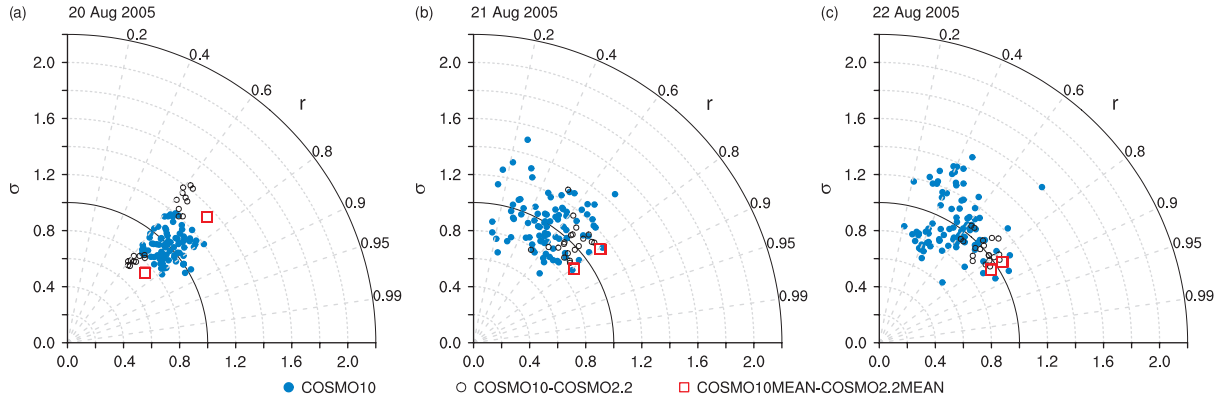

Figure 6. Taylor diagrams of daily accumulated precipitation obtained on (a) 20 August 2005 (1200 to 0600 UTC), (b) 21 August 2005 (0600 to 0600 UTC), and (c) 22 August 2005 (0600 to 0600 UTC) for the whole computational domain. Solid and open circles compare the COSMO10 members among themselves and the COSMO10 against the corresponding COSMO2.2 members, respectively, while the squares refer to the two ensemble means. The 2.2 km integrations have been averaged on the 10 km grid for comparison. By construction (i.e. both the pairs (m_1, m_2) and (m_2, m_1) are considered), the points are mirrored along $\sigma = 1$. This figure is available in colour online at www.interscience.wiley.com/qj

where N denotes the number of grid points and the overbar an area-mean value. Two identical simulations will lie on the reference point.

The solid and open circles in Figure 6 compare the COSMO10 members among themselves and the COSMO10 against the corresponding COSMO2.2 members, respectively, while the squares refer to the two ensemble means. Figure 6(a) shows that on the first day, the correlation between a 2.2 km simulation (or ensemble mean) and its 10 km counterpart is smaller than between two 10 km members. The normalized rms difference E and the ratio of their standard deviations σ are also larger. Hence, decreasing the model mesh size induces larger differences than generating a synoptic-scale ensemble, at least in the metric considered. On the second and third days, the correlations between corresponding COSMO2.2 and COSMO10 members are generally higher than between different 10 km simulations. As a consequence, most of the 10 km integrations are more akin to their 2.2 km version than to any other ensemble member. This effect mostly follows from the strongly decreasing correlations between COSMO10 simulations after the first day (full circles in Figures 6(a,b)), which itself follows from the increasing ensemble spread with increasing lead time. Finally the squares in Figure 6 indicate that the correlations between the COSMO2.2 and COSMO10 ensemble means are especially high and higher than between any two integrations, as expected from the smoothing effect of the averaging process (Section 4.3).

4.2. Forecast probabilities

Figure 7 shows probability maps of 24-hour accumulated precipitation exceeding 100 mm as derived with COSMO2.2 and COSMO10 for 21 and 22 August. The 2.2 km and 10 km probability maps agree with each other and predict the occurrence of heavy rainfalls in an elongated band north of the Alps. The signal is weaker in COSMO2.2 than in COSMO10 on 21 August (Figures 7(a,c)), but the localization is more accurate. On 22 August, COSMO2.2 yields higher probabilities than COSMO10 and thus provides better guidance, although both ensembles only weakly suggest the occurrence of heavy rainfalls over Austria (Figures 7(b,d) and 5(c)).

Figure 8 shows time series of precipitation with interquartile range averaged over the three subdomains JU, CS, and ES (Figure 1(b)). The observations again attest the generally high skill of the 2.2 km and 10 km medians. Also, the observational curve lies in the interquartile range except on 20 August (domains CS and ES) and around 12 UTC on 21 August in COSMO2.2 (domain ES).

Comparison of the interquartile ranges reveals that, with the exception of the first ∼30 h over JU, the two ensembles do overlap. No systematic tendency of the 2.2 km integrations to induce a larger spread can be recognized. Theoretically, a larger spread would have been expected with a finer grid spacing. Computing a domain-mean value hides parts of this effect.

4.3. Dynamical interpretation

The previous two sections have documented on the one hand that COSMO2.2 is able to outperform COSMO10, especially by providing a more accurate localization of the region experiencing heavy rainfalls on 21 August. On the other hand, COSMO10 yields better results on 20 August. Also, even if the differences between COSMO2.2 and COSMO10 may be locally large, the two ensembles bear strong similarities in terms of means and probabilities. The question arises, whether the latter findings are conditioned by the synoptic situation or by the experimental set-up. These issues are examined here in more detail and may allow some generalization of our results. In particular, we analyze the results with the aim of isolating the role of convective precipitation and of the orographic representation, as they constitute the main differences between COSMO2.2 and COSMO10 (Section 2).

DOI: 10.1002/qj

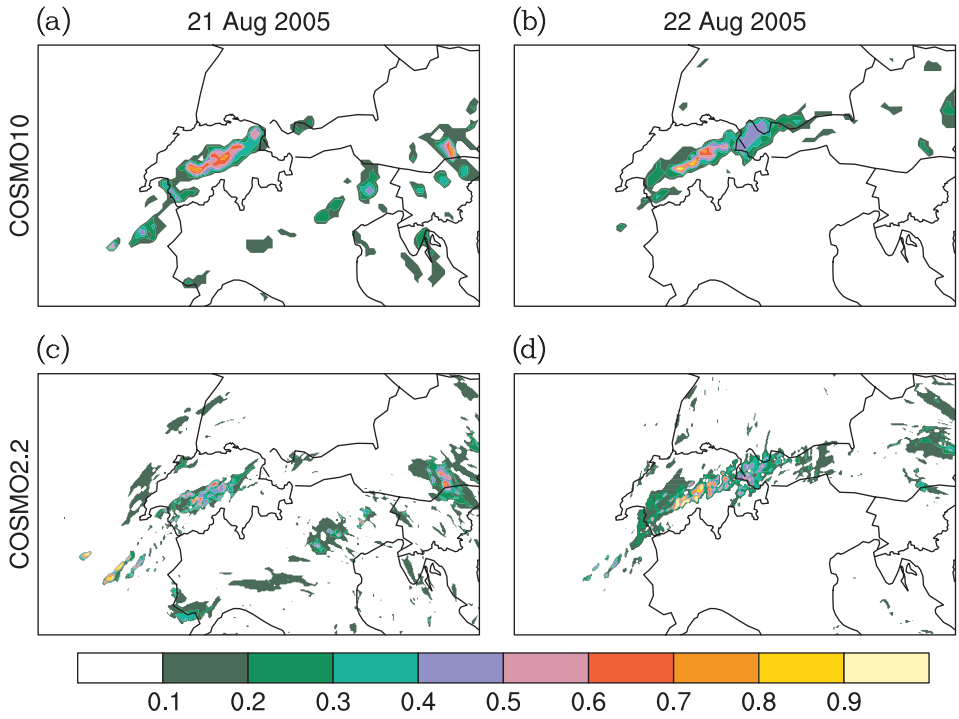

Figure 7. Probability maps derived with (a,b) COMSO10 and (c,d) COSMO2.2: probabilities that the accumulated (0600 to 0600 UTC) precipitation on (a,c) 21 August 2005 and (b,d) 22 August 2005 exceeds 100 mm.

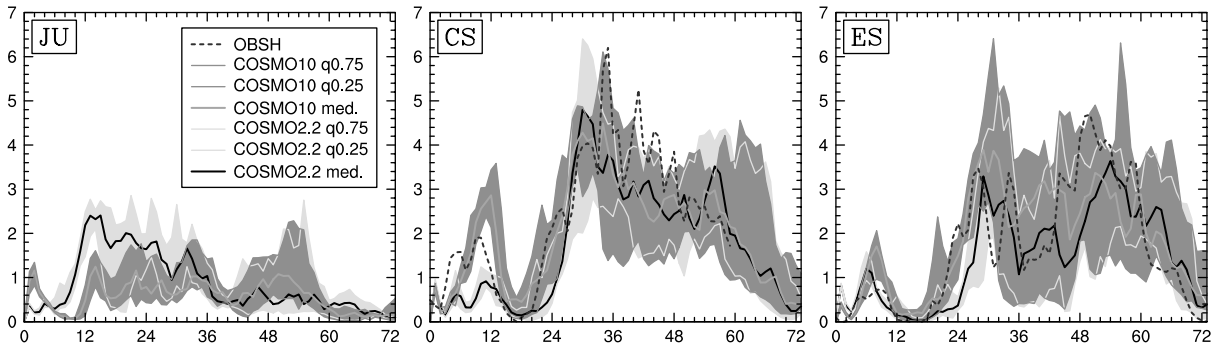

Figure 8. Time series of precipitation (mm h^{-1}) averaged over the three subdomains JU, CS, and ES (marked in Figure 1(b)) obtained with COSMO2.2, COSMO10, and observations OBSH. The interquartile ranges (25%–75%) and the medians are shown. The observational curve is masked in cases of missing radar information. The simulations start on 1200 UTC on 20 August 2005, and time is in hours.

Figures 9(a–f) show ensemble-mean stratiform and convective precipitation simulated by COSMO10 for 20, 21 and 22 August. Note that the partitioning between convective and stratiform rain is parametrized and cannot be validated against observations. The lower row contains maps of ensemble-mean accumulated precipitation resulting from COSMO2.2T10 integrations. This ensemble uses cloud-resolving resolution but a smoothed topography roughly corresponding to that of COSMO10 (Table I and Section 2.3).

Comparison of the different panels reveals that the sensitivity of the simulated precipitation to the topography and to the convective representation depends upon the simulated day and thus upon the overall synoptic situation. On 20 August, the use of a pseudo-10 km topography at 2.2 km horizontal resolution alters the spatial rainfall distribution over Switzerland and produces a pattern similar to COSMO10 (compare Figure 9(g) against Figures 5(d,g) and the observations in Figure 5(a)). It is thus the orographic representation that explains the differences between COSMO10 and COSMO2.2. On 21 and 22 August (Figures 5(h,i), 9(h,i)), the specifics of the chosen topography merely affect the rain amounts obtained over the mountain peaks and the spatial precipitation variability. As expected, the sharper 2.2 km version yields higher precipitation maxima (especially on the Massif Central in Figures 9(h) and 5(h)). However, the impact on the simulated large-scale precipitation distribution remains rather small. The spatial correlation computed between COSMO2.2 and COSMO2.2T10 amounts here to about 0.9 for 21 and 22 August against 0.8 for 20 August.

It should be noted that the better agreement of COSMO2.2T10 with the observations on 20 August does not imply that coarser-resolution terrain may have better

DOI: 10.1002/qj

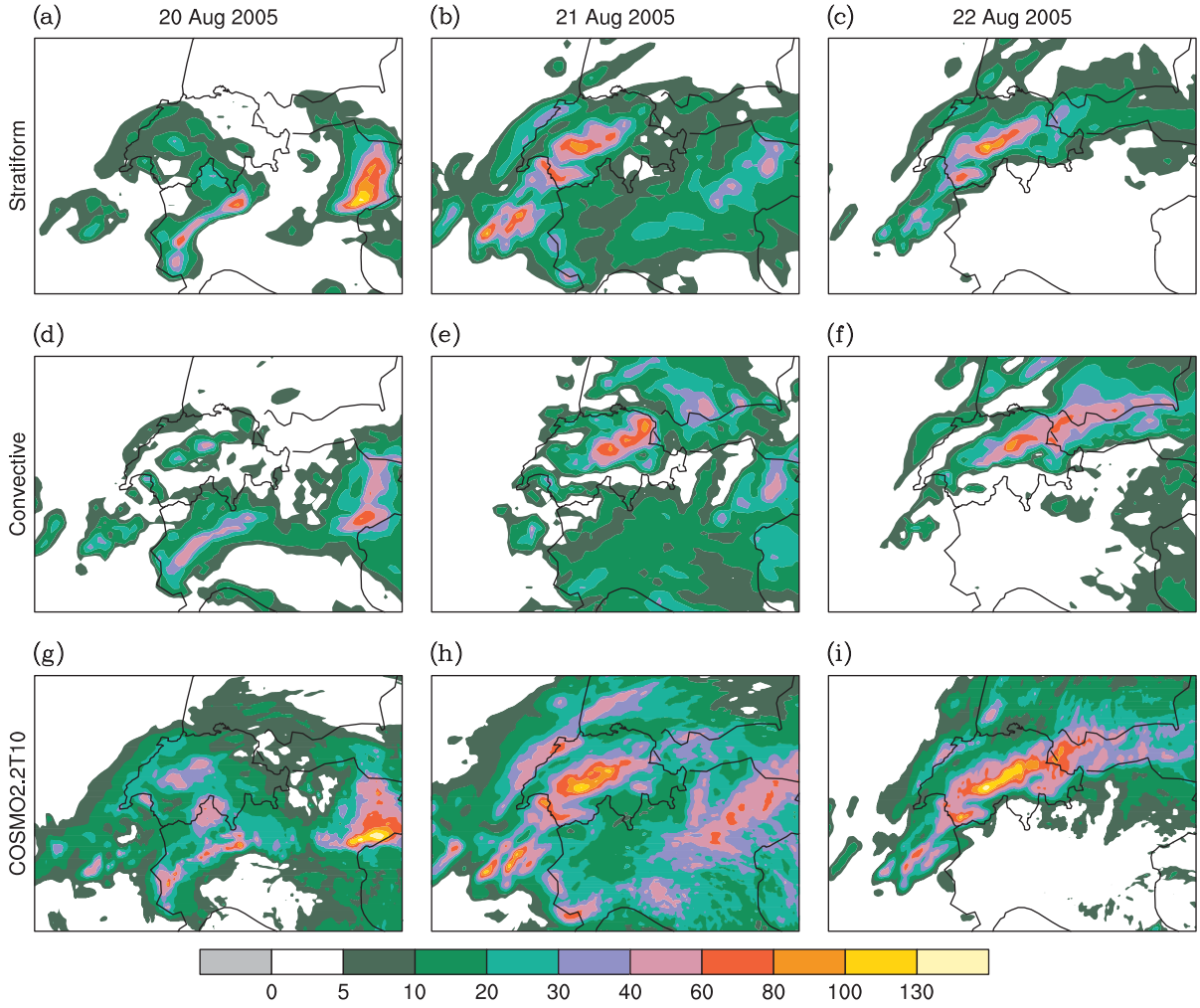

Figure 9. Ensemble-mean (a–c) stratiform and (d–f) convective precipitation (mm) obtained with COSMO10 and (g–i) ensemble mean total precipitation (mm) derived from COSMO2.2T10. Times are as in Figure 5.

QPF results. For instance, the opposite situation occurs on 21 and 22 August. Comparison of Figures 5 and 9 merely indicates that, depending on the synoptic situation, a small change in the orographic forcing can have a significant effect on the simulated precipitation. Similar sensitivities have been obtained in other studies utilizing deterministic real or idealized simulations (e.g. Cosma *et al*., 2002; Zängl, 2007b) and would in fact speak for the use of realistic topography and thus high-resolution integrations.

Concerning the role of moist convection in explaining the precipitation differences (respectively, the simulation similarities), Figures 9(d–f) reveal that, depending on the region, substantial amounts of precipitation fall as convective precipitation in COSMO10. This is in agreement with the cloud-resolving simulations which exhibited conditional instability below 700 hPa (e.g. Figure 4 and Section 3). However, comparison of Figures 5(d–f) with Figures 9(g–i) surprisingly indicates that the presence of moist convection does not induce large precipitation differences between COSMO2.2 and COSMO10, as may have been expected (Section 1). The exception is 21 August, where the spurious COSMO10 rain peak visible over northeastern Switzerland is clearly produced by the Tiedtke mass flux scheme.

Reasons for the different sensitivities with time of the simulated large-scale precipitation to the details of the chosen topography and to the presence of moist convective instabilities are further investigated with Figure 10. It shows ensemble-mean horizontal moisture fluxes and wind vectors at 850 hPa in COSMO2.2 and COSMO2.2T10 averaged on 20, 21 and 22 August 2005. On 20 August, the location, extent and strength of the low-level jet carrying high moisture towards the Alps are highly sensitive to the orographic representation. The pseudo-10 km topography in COSMO2.2T10 allows higher moisture flux on the northern Alpine slopes and shifts the flow direction from parallel to slightly against the Alps. As a consequence, precipitation falls over central Switzerland in COSMO2.2T10 (and COSMO10) in place of the Jura region in COSMO2.2. This explains much of the differences seen in Figures 9 and 5. The observed change in low-level flow may be related to a change from a regime with blocked low-level flow in COSMO2.2 to a partially 'flow-over' regime in COSMO2.2T10. It is well known from theoretical

DOI: 10.1002/qj

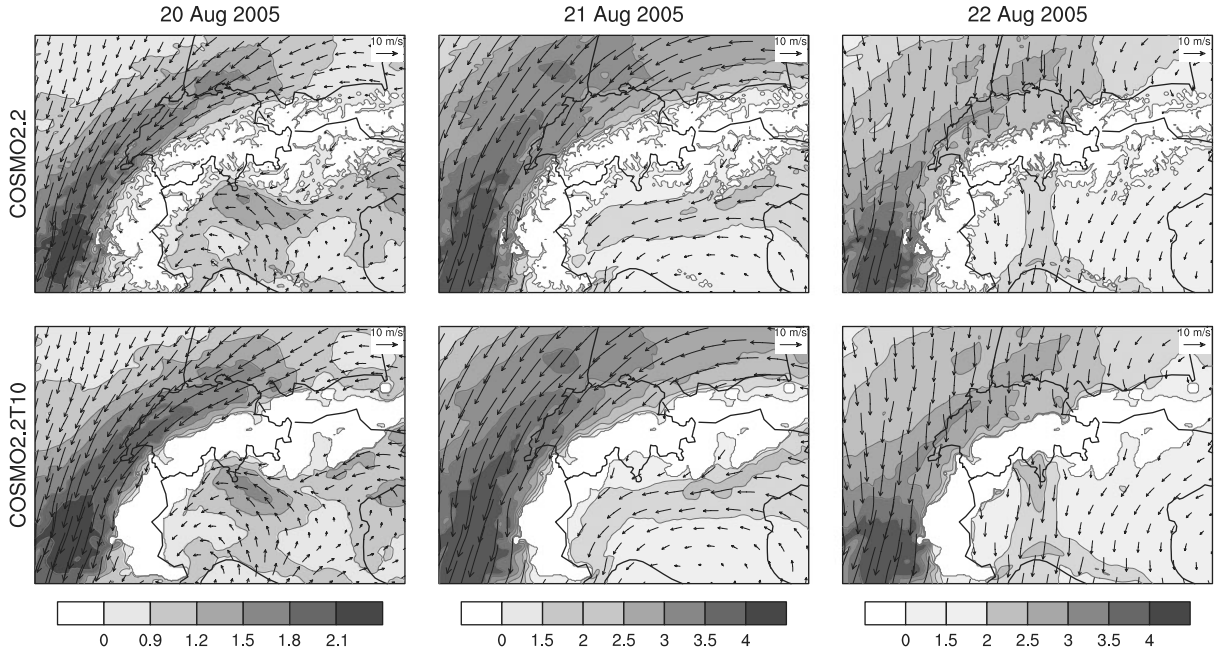

Figure 10. Ensemble-mean horizontal moisture flux (shading, kg m^{-2} s^{-1}) and wind vectors (m s^{-1}) obtained in COSMO2.2 and COSMO2.2T10 at 850 hPa averaged over 20 (1200 UTC to 0600 UTC), 21 (0600 UTC to 0600 UTC), and 22 (0600 UTC to 0600 UTC) August 2005.

and idealized studies that these flow regimes critically depend upon the upstream wind profile and the height of the underlying mountain barrier (Smith and Gronas, 1993; Schär and Durran, 1997). On 21 August, moisture fluxes and wind vectors agree in both ensembles for three reasons. First, as the low pressure system moves eastward with time (e.g. Figure 2), the wind arrows rotate anticlockwise. The new cyclone location implies a flow against the Alps, so that a slight shift in its direction or strength produces a weaker impact on the simulated precipitation. Second, differences in the position of the low-level jet do exist between individual members (and consequently in precipitation, e.g. Figure 6), but they are overpowered by the increased ensemble spread (not shown). Third, the winds on 21 August are stronger than on 20 August, allowing some flow-over also with the 2.2 km topography. On 22 August, all these factors are amplified. This reduces with time the sensitivity of the simulated large-scale precipitation to the details of the chosen topography as observed in Figures 9 and 5.

Similar considerations hold for the role of moist convection. On 20 August, potential differences between COSMO2.2 and COSMO10 due to the Tiedtke mass flux scheme are overpowered by the shift in the low-level jet position. On 22 August, the observed strong flow, which perpendicularly impinges upon the Alps (Figure 10), seems to enforce the location of precipitation independently of the presence of convective instabilities. Also, the ensemble spread tends to smooth out the randomness associated with convective cells (e.g. Kong *et al*., 2006). As such, differences between COSMO2.2 and COSMO10 remain mainly visible on 21 August.

In conclusion, the resolution-induced differences critically depend upon the simulated synoptic situation, the interaction of the flow with the topography, and indirectly upon the chosen integration domain. For the simulated event, the combination of these effects allowed for two phases (20 and 21 August) with larger and one phase (22 August) with smaller differences between the two ensembles. There are thus prospects that, depending on the simulated synoptic situation, the use of a cloud-resolving EPS may be beneficial. Such findings are consistent with results obtained with deterministic integrations (e.g. Warner *et al*., 1997; Mass *et al*., 2002; Zängl, 2007b). However, in contrast to these studies, the use of an ensemble reduces the impact of higher grid spacing. Although lower-resolution members cannot include small-scale variability and correctly capture moist convection, their spread already imitates some of the resolution-induced effects. In particular, a shift in wind direction, as observed in Figure 10, may follow either from a modification in orographic forcing (embedded to the model mesh size) or from a change in the location of the cyclone centre (as sampled by distinct members). Moreover, the increase in ensemble spread with increasing lead time tends to overpower differences which may have existed between individual low- and high-resolution integrations. The dependence on the ensemble spread makes the hypothetical gain achieved by cloud-resolving resolution sensitive to the chosen lead time.

5. Role of initial versus lateral boundary uncertainties

In this section, we investigate the sensitivity of the cloud-resolving simulations to initial and lateral boundary uncertainties. We first compare the COSMO2.2 against the COSMO2.2INI ensemble. In contrast to COSMO2.2,

DOI: 10.1002/qj

COSMO2.2INI uses identical lateral boundary conditions (Section 2.3 and Table I). The comparison of these ensembles allows us to quantify the contribution of the initial uncertainties to the ensuing ensemble spread.

Figure 11 shows interquartile ranges obtained with COSMO2.2 and COSMO2.2INI for the three subdomains JU, CS, and ES, plotted in a fashion similar to Figure 8. The lower panels contain the corresponding ratios. Qualitatively similar results can be derived by considering the whole range (i.e. maximum−minimum, not shown).

During the first ∼12 hours, the interquartile ranges of COSMO2.2 and COSMO2.2INI are of similar magnitude. The generated ensemble spread is thus dominated by the amplification of initial uncertainties. From 12 hours to about 55 hours (domain JU), 60 hours (CS), and 62 hours (ES), the contribution of the initial uncertainties oscillates between about 20% and 50% with occasional stronger/weaker peak values. Afterwards, the COSMO2.2INI interquartile range becomes negligible. Thus overall we observe a transition from a period dominated by initial uncertainties to one dominated by lateral boundary conditions.

The predominance of initial over lateral boundary uncertainties during the first 12 hours is due to the memory of the simulations with respect to their initial perturbations, i.e., the time needed for the lateral boundary perturbations to affect the whole integration domain. For comparison, Frogner and Iversen (2002) found a time period of 12 to 24 hours (in terms of the 500 hPa geopotential height) for limited-area simulations using a ∼28 km grid spacing. Later, the different evolution in Figure 11 of the interquartile ranges in COSMO2.2 and COSMO2.2INI highlights the distinctive nature of the underlying amplification processes. As documented in previous predictability studies (e.g. Hohenegger *et al.*, 2006), the use of identical lateral boundary conditions as in COSMO2.2INI constrains error growth to the presence of moist convection, where significant amplification is favoured under weak flow regimes. The presence of both convective instability and stratiform precipitation as well as moderate-to-strong winds explain the moderate COSMO2.2INI spread in the second phase of the simulations. The arrival of strong winds on the back of the precipitating system (e.g. Figure 10) then prevents any divergence among the simulations towards the end of the integrations as domain-internal errors are rapidly flushed away (Hohenegger *et al.*, 2006). In contrast, perturbing both initial and lateral boundary conditions in COSMO2.2 allows larger-scale error growth controlled by the lateral boundaries.

As final step, we test the role of the particular choice of the initial perturbations within ensembles that utilize identical lateral boundary conditions. To this end we employ ensemble SHIFT2.2 that is derived from a shifting initialization strategy and that uses otherwise the same set-up as COSMO2.2INI (Section 2.3 and Table I). The initial perturbations of the two ensembles differ fundamentally. They are dominated, respectively, by synoptic-scale structures (COSMO2.2INI) and small-scale noise (SHIFT2.2).

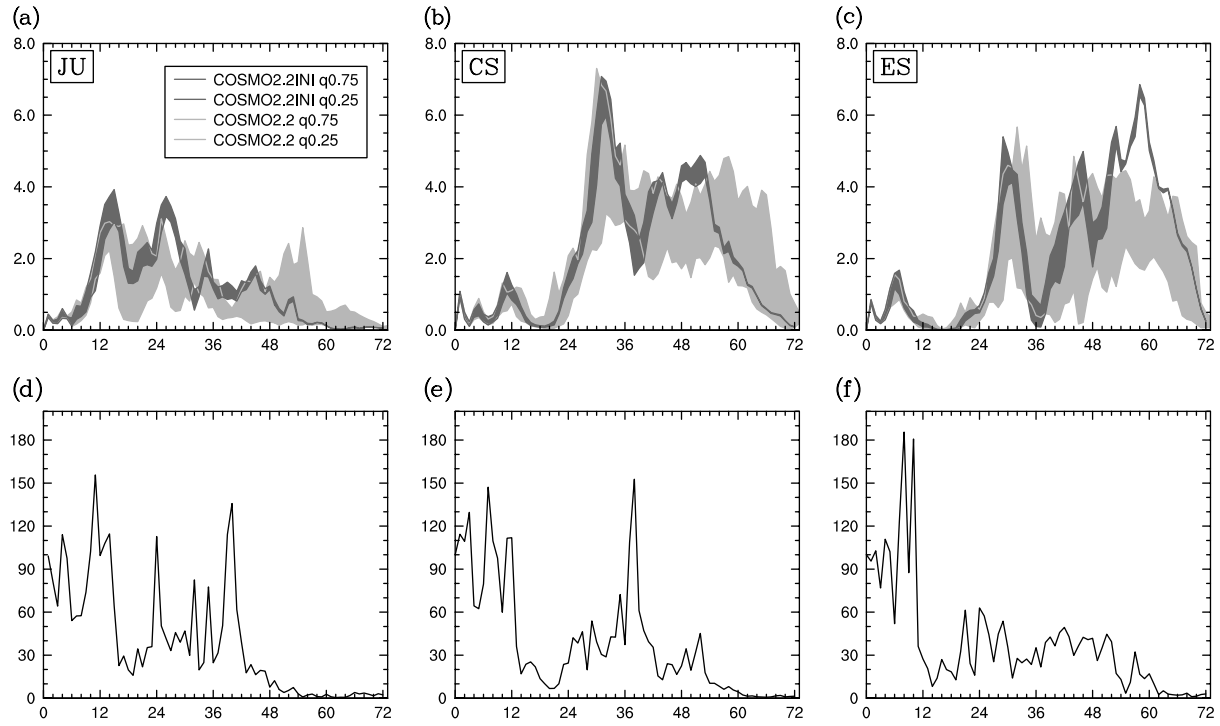

Figure 11. Time series of interquartile precipitation range (mm h^{-1}) averaged over the three subdomains (a) JU, (b) CS, and (c) ES for COSMO2.2 and COSMO2.2INI. (d)–(f) show the corresponding ratios (%) between COSMO2.2INI and COSMO2.2 interquartile ranges. The simulations start on 1200 UTC 20 August 2005. Time is in hours.

DOI: 10.1002/qj

As SHIFT2.2 has merely four members (to minimize the time delay induced by the shifting initialization technique; Section 2.3), we compare it against a subset of COSMO2.2INI referred to as COSMO2.2INIsub. Figure 12 shows maps of associated ensemble-mean accumulated precipitation and normalized spread. The maps refer to 20 August where we expect the strongest influence of the chosen initial perturbations (e.g. Hohenegger and Schär, 2007a). Consideration indicates that SHIFT2.2 and COSMO2.2INIsub yield qualitatively a similar ensemble mean (Figures 12(a,c)) and comparable normalized spread of accumulated precipitation (Figures 12(b,d)).

More detailed consideration of Figures 12(b,d) shows that the shifting initialization technique yields a larger normalized spread than the downscaled singular vectors, in particular in the precipitation centres over northern Italy. We believe that this is primarily due to the fact that the small-scale initial perturbations of SHIFT2.2 may grow faster, and that they have (despite representing design uncertainties) larger initial amplitudes than the downscaled singular vectors.

6. Conclusions

The performance of a cloud-resolving (2.2 km) ensemble prediction system has been assessed against its driving lower-resolution (10 km) limited-area EPS (COSMO-LEPS) for a case of heavy precipitation over the Alpine region. The chosen case is the August 2005 Alpine flood that caused damage of the order of 3.3 billion US$. The initial and lateral boundary perturbations originate from the global ECMWF EPS and are dynamically downscaled to 10 km and 2.2 km. The cloud-resolving EPS explicitly resolves deep convection and exhibits higher-resolution (more realistic) surface fields. In a second step, the sensitivity of the cloud-resolving integrations to the representation of initial and lateral boundary uncertainties has been investigated. For this purpose, EPS using perturbed initial conditions but identical lateral boundary conditions have been generated. The considered sampling strategies include the dynamically downscaled singular vectors (as in COSMO-LEPS) and a shifting initialization technique (that generates small-scale perturbations). All the ensembles assume a perfect model.

The cloud-resolving EPS and COSMO-LEPS are both very skilful at capturing the phase of heavy precipitation which occurred on 21 and 22 August 2005 over central Switzerland, both in terms of means and probabilities. The cloud-resolving EPS outperforms COSMO-LEPS on 21 August, where the latter produces unrealistically high rainfalls over northeastern Switzerland. On 22 August, the two ensembles perform comparably. On 20 August, before the actual phase of heavy rain, the cloud-resolving EPS misplaces the precipitation maximum and appears less skilful than COSMO-LEPS. Except on that day, the resolution-induced differences tend to be smaller than typical member-to-member variability.

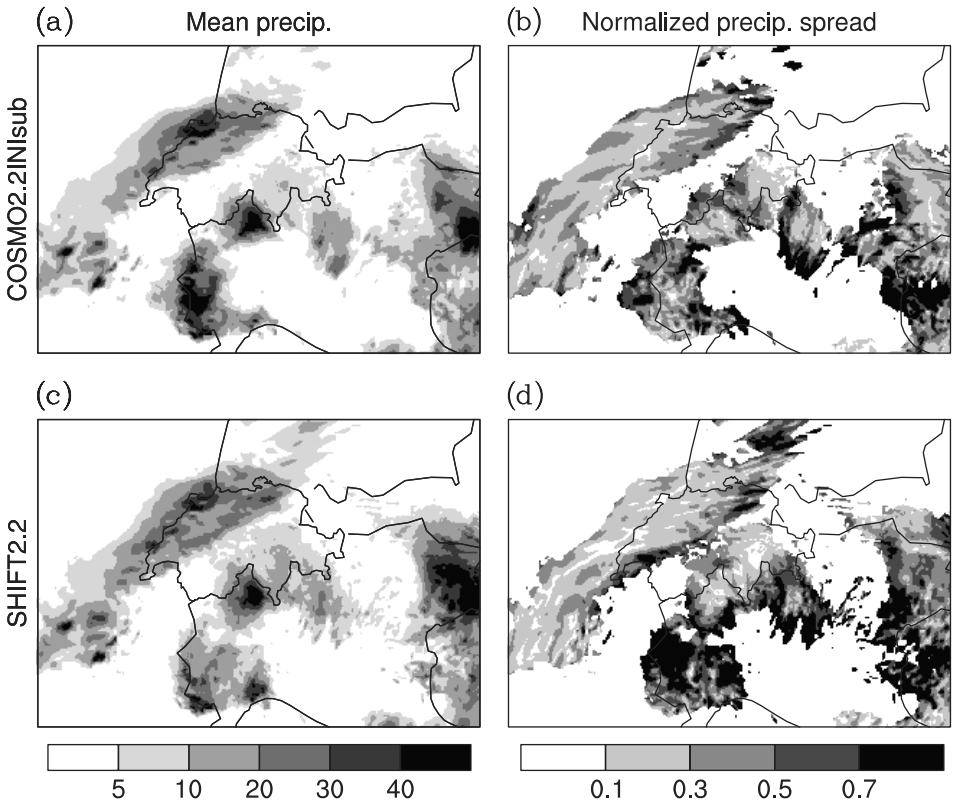

Figure 12. (a) ensemble-mean (mm) and (b) normalized precipitation spread in COSMO2.2INIsub obtained on 20 August 2005 (from 1600 UTC to 0600 UTC). (c,d) are as (a,b), but for SHIFT2.2. The normalized precipitation spread in (b,d) is computed at locations where the ensemble mean accumulated precipitation exceeds 5 mm.

DOI: 10.1002/qj

The differences between the two ensembles (respectively their high similarities) can be tied to the overall synoptic situation (stratiform versus convective precipitation, location of the low pressure centre), to the interaction of the flow with the topography, and to the experimental set-up (lead time and integration domain). On 20 August, the misplacement of the precipitation peak in the cloud-resolving EPS compared with COSMO-LEPS relates to orographic effects. A change in the orographic representation is able to affect the strength, location, and direction of the low-level jet and thereby to significantly affect the precipitation distribution. The details of this sensitivity depend upon the location of the low pressure centre, the position of the lateral boundaries, and the relatively small ensemble spread (first integration day). Later on 21 and 22 August, the increased ensemble spread, the anticlockwise rotation of the flow towards the Alps due to the eastward propagation of the cyclone centre, and the overall stronger low-level jet yield a reduced sensitivity. Simulated precipitation differences then mainly relate to the treatment of moist convection. Even if convective instabilities are present in the simulations, they do not cause COSMO2.2 to diverge from COSMO10 (especially on 22 August) due to the increasing ensemble spread. Also, the presence of a strong low-level jet which impinges perpendicularly on the main mountain barrier seems to enforce the precipitation location.

In terms of ensemble spread, the amplification of initial perturbations dominates over lateral boundary uncertainties during the first $\sim$12 hours of the cloud-resolving integrations. During this time, the ensemble members also show a pronounced sensitivity to the characteristics of the initial perturbations. The use of the shifting initialization technique instead of the downscaled singular vectors yields a larger precipitation spread. Afterwards, the divergence among the cloud-resolving simulations is controlled by large-scale error growth advected from the boundaries into the computational domain. Locally, the growth of initial disturbances may be large, but such effects tend to be limited because of the presence of both stratiform and convective precipitation as well as strong winds flushing away domain-internal errors. This may have further contributed to the high skill of the two ensembles.

Our study investigated one real case only. Given the strong dependence of the resolution-induced differences upon the considered event, a strong case-to-case variability is expected. It is positive to note that, despite the overall small differences, the cloud-resolving ensemble yields results as good as and even better than its driving lower-resolution EPS, at least for two out of the three simulated days. Further studies would be needed to assess the performance of such high-resolution ensembles for a wide range of synoptic situations. Based on our results, it is likely that the generation of an ensemble reduces the possible gain achieved by higher model mesh sizes compared with deterministic high-resolution integrations.

Another prospect for cloud-resolving EPS concerns their coupling to hydrological models. Probabilistic hydrological forecasts have higher skill than deterministic ones (e.g. Verbunt *et al*., 2007) and require meteorological inputs of high horizontal resolution (e.g. Benoit *et al*., 2003). The potential benefits of a cloud-resolving EPS over a lower-resolution EPS for probabilistic flood forecasting are the subject of another currently ongoing study related to the devastating August 2005 flood.

Acknowledgements

The numerical simulations were performed on the CRAY XT-3 at the Swiss National Supercomputing Centre (CSCS) and on the IBM cluster of ECMWF. The authors would like to thank MeteoSwiss, Christoph Frei and Marc Wüest for providing the observational data, Reinhard Schiemann and Bodo Ahrens for constructive discussions, as well as the two reviewers for helpful comments. This study was partly supported by the Swiss National Science Foundation through the National Centre for Competence in Research (NCCR-Climate).

References

Baldauf M, Schulz J. 2004. Prognostic precipitation in the Lokal Modell (LM) of DWD. *COSMO Newsletter* **4**: 177–180. http://www.cosmo-model.org.

Benoit R, Schär C, Binder P, Chamberland S, Davies HC, Desgagné M, Girard C, Keil C, Kouwen N, Lüthi D, Maric D, Müller E, Pellerin P, Schmidli J, Schubiger F, Schwierz C, Sprenger M, Walser A, Willemse S, Yu W, Zala E. 2002. The real-time ultrafinescale forecast support during the Special Observing Period of the MAP. *Bull. Am. Meteorol. Soc.* **83**: 85–109.

Benoit R, Kouwen N, Yu W, Chamberland S, Pellerin P. 2003. Hydrometeorological aspects of the real-time ultrafinescale forecast support during the Special Observing Period of the MAP. *Hydrol. Earth System Sci.* **7**: 877–889.

Bezzola GR, Hegg C. (eds.) 2007. *Ereignisanalyse Hochwasser 2005. Teil 1 – Prozesse, Schäden und erste Einordnung*. Bundesamt für Umwelt BAFU, Bern, Eidgenössische Forschungsanstalt WSL: Birmensdorf. http://www.wsl.ch/publikationen/books/7970_DE.

BMLFUW (Bundesministerium für Land- und Forstwirtschaft, Umwelt und Wasserwirtschaft). 2006. *Hochwasser 2005: Ereignisdokumentation.* Bericht der Bundeswasserbauverwaltung, des Forsttechnischen Dienstess für Wildbach- und Lawinenverbauung und des Hydrographischen Dienstes: Wien. http://gpool.lfrz.at/gpool/main.cgi?rq=ed&etid=38&eid=965&oid=234&th=1.

Brooks HE, Doswell CA, Maddox RA. 1992. On the use of mesoscale and cloud-scale models in operational forecasting. *Weather Forecasting* **7**: 120–132.

Buizza R, Miller M, Palmer TN. 1999. Stochastic simulation of model uncertainties. *Q. J. R. Meteorol. Soc* **125**: 2887–2908.

Buizza R, Houtekamer PL, Toth Z, Pellerin G, Wei M, Zhu Y. 2005. A comparison of the ECMWF, MSC, and NCEP global ensemble prediction systems. *Mon. Weather Rev.* **133**: 1076–1097.

Buzzi A, Tartaglione N, Malguzzi P. 1998. Numerical simulations of the 1994 Piedmont flood: Role of orography and moist processes. *Mon. Weather Rev.* **126**: 2369–2383.

Buzzi A, Davolio S, D'Isidoro M, Malguzzi P. 2004. The impact of resolution and of map reanalysis on the simulations of heavy precipitation during map cases. *Meteorol. Zeitschrift* **13**: 91–97.

Christensen JH, Christensen OB. 2003. Severe summertime flooding in Europe. *Nature* **421**: 805–806.

Colle BA, Wolfe JB, Steenburgh WJ, Kingsmill DE, Cox JAW, Shafer JC. 2005. High-resolution simulations and microphysical validation of an orographic precipitation event over the Wasatch mountains during IPEX IOP3. *Mon. Weather Rev.* **133**: 2947–2971.

Cosma S, Richard E, Miniscloux F. 2002. The role of small-scale orographic features in the spatial distribution of precipitation. *Q. J. R. Meteorol. Soc.* **128**: 75–92.

Davies HC. 1976. A lateral boundary formulation for multi-level prediction models. *Q. J. R. Meteorol. Soc.* **102**: 405–418.

DOI: 10.1002/qj

Doms G, Förstner J. 2004. Development of a kilometer-scale NWP-System: LMK. *COSMO Newsletter* **4**: 159–167. http://www.cosmo-model.org.

Ducrocq V, Ricard D, Lafore JP, Orain F. 2002. Storm-scale numerical rainfall prediction for five precipitating events over France: On the importance of the initial humidity field. *Weather Forecasting* **17**: 1236–1256.

Durran DR, Klemp JB. 1982. On the effects of moisture on the Brunt–Väisälä frequency. *J. Atmos. Sci.* **39**: 2152–2158.

Ebert EE, Damrath U, Wergen W, Baldwin ME. 2003. The WGNE assessment of short-term quantitative precipitation forecasts. *Bull. Am. Meteorol. Soc.* **84**: 481–492.

Eckel FA, Mass CF. 2005. Aspects of effective mesoscale, short-range ensemble forecasting. *Weather Forecasting* **20**: 328–350.

Frei C. 2006. *Eine Länder übergreifende Niederschlags-Analyse zum August-Hochwasser 2005. Ergänzung zu Arbeitsbericht 211. Arbeitsbericht* 213. MeteoSchweiz: Zürich. http://www.meteoschweiz.admin.ch/web/de/klima/aktuelle_berichte/hochwasser_2005.html.

Frei C, Schär C. 1998. A precipitation climatology of the Alps from high-resolution rain-gauge observations. *Int. J. Climatol.* **18**: 873–900.

Frei C, Schöl R, Fukutome S, Schmidli J, Vidale PL. 2006. Future change of precipitation extremes in Europe: An intercomparison of scenarios from regional climate models. *J. Geophys. Res.* **11**: DOI: 10.1029/2005JD005965.

Fritsch JM, Carbone RE. 2004. Improving quantitative precipitation forecasts in the warm season – A USWRP research and development strategy. *Bull. Am. Meteorol. Soc.* **85**: 955–964.

Frogner IL, Iversen T. 2002. High-resolution limited-area ensemble predictions based on low-resolution targeted singular vectors. *Q. J. R. Meteorol. Soc.* **128**: 1321–1341.

Fuhrer O, Schär C. 2005. Embedded cellular convection in moist flow past topography. *J. Atmos. Sci.* **62**: 2810–2828.

Grimit EP, Mass CF. 2002. Initial results of a mesoscale short-range ensemble forecasting system over the Pacific Northwest. *Weather Forecasting* **17**: 192–205.

Heise E, Lange M, Ritter B, Schrodin R. 2003. Improvement and validation of the multi-layer soil model. *COSMO Newsletter* **3**: 198–203. http://www.cosmo-model.org.

Hohenegger C, Lüthi D, Schär C. 2006. Predictability mysteries in cloud-resolving models. *Mon. Weather Rev.* **134**: 2095–2107.

Hohenegger C, Schär C. 2007a. Predictability and error growth dynamics in a cloud-resolving model. *J. Atmos. Sci.* **64**: 4467–4478.

Hohenegger C, Schär C. 2007b. Atmospheric predictability at synoptic versus cloud-resolving scales. *Bull. Am. Meteorol. Soc.* **11**: 1783–1793.

Jaun S, Ahrens B, Walser A, Ewen T, Schär C. 2008. A probabilistic view on the August 2005 floods in the upper Rhine catchment. *Nat. Hazard Earth Sys. Sci.* **8**: 281–291.

Kalnay E. 2003. *Atmospheric modeling, data assimilation and predictability*. Cambridge University Press: Cambridge, UK.

Kanonier J. 2006. *Das Starkregen- und Hochwasserereignis des August 2005 in Vorarlberg*. Ein Bericht des Amts der Vorarlberger Landesregierung: Feldkirch. http://www.vorarlberg.at/pdf/naturereignis-dokumentatio.pdf.

Kaufmann P, Schubiger F, Binder P. 2003. Precipitation forecasting by a mesoscale numerical weather prediction (nwp) model: Eight years of experience. *Hydrol. Earth System Sci.* **7**: 812–832.

Keil C, Volkert H, Majewski D. 1999. The Oder flood in July 1997: Transport routes of precipitable water diagnosed with an operational forecast model. *Geophys. Res. Lett.* **26**: 235–238.

Klein Tank AMG, Können GP. 2003. Trends in indices of daily temperature and precipitation extremes in Europe, 1946–1999. *J. Climate* **16**: 3665–3680.

Klemp J, Wilhelmson R. 1978. Simulation of 3-dimensional convective storm dynamics. *J. Atmos. Sci.* **35**: 1070–1096.

Kong FY, Droegemeier K, Hickmon N. 2006. Multiresolution ensemble forecasts of an observed tornadic thunderstorm system. Part I: Comparison of coarse- and fine-grid experiments. *Mon. Weather Rev.* **134**: 807–833.

Kong FY, Droegemeier KK, Hickmon NL. 2007. Multiresolution ensemble forecasts of an observed tornadic thunderstorm system. Part II: Storm-scale experiments. *Mon. Weather Rev.* **135**: 759–782.

LFU (Landesamt für Umwelt). 2006. *August-Hochwasser 2005 in Südbayern*. Arbeitsbericht der Bayerischen Landesamt für Umwelt. http://www.hnd.bayern.de/ereignisse/hw220 805/hw200 508_end-bericht.pdf.

Marsigli C, Montani A, Nerozzi F, Paccagnella T, Tibaldi S, Molteni F, Buizza R. 2001. A strategy for high-resolution ensemble prediction. II: Limited-area experiments in four alpine flood events. *Q. J. R. Meteorol. Soc.* **127**: 2095–2115.

Marsigli C, Montani A, Nerozzi F, Paccagnella T. 2004. Probabilistic high-resolution forecast of heavy precipitation over Central Europe. *Nat. Hazard Earth Sys. Sci.* **4**: 315–322.

Marsigli C, Boccanera F, Montani A, Paccagnella T. 2005. The cosmo-leps mesoscale ensemble system: validation of the methodology and verification. *Nonlinear Proc. Geophys.* **12**: 527–536.

Mass CF, Ovens D, Westrick K, Colle BA. 2002. Does increasing horizontal resolution produce more skillful forecasts? *Bull. Am. Meteorol. Soc.* **83**: 407–430.

Mellor GL, Yamada T. 1982. Development of a turbulence closure model for geophysical flow problems. *Rev. Geophys. Space Phys.* **20**: 831–857.

MeteoSchweiz. 2006. *Starkniederschlagsereignis August 2005. Arbeitsbericht* 211, MeteoSchweiz: Zürich.

Molteni F, Buizza R, Palmer TN, Petroliagis T. 1996. The ECMWF ensemble prediction system: Methodology and validation. *Q. J. R. Meteorol. Soc.* **122**: 73–119.

Molteni F, Buizza R, Marsigli C, Montani A, Nerozzi F, Paccagnella T. 2001. A strategy for high-resolution ensemble prediction. I: Definition of representative members and global-model experiments. *Q. J. R. Meteorol. Soc.* **127**: 2069–2094.

Montani A, Marsigli C, Nerozzi F, Paccagnella T, Tibaldi S, Buizza R. 2003. The Soverato flood in southern Italy: Performance of global and limited-area ensemble forecasts. *Nonlinear Proc. Geophys.* **10**: 261–274.

Nutter PJ, Stensrud D, Xue M. 2004. Effects of coarsely resolved and temporally interpolated lateral boundary conditions on the dispersion of limited-area ensemble forecasts. *Mon. Weather Rev.* **132**: 2358–2377.

Petrow T, Thieken AH, Kreibich H, Bahlburg CH, Merz B. 2006. Improvements on flood alleviation in Germany: Lessons learned from the Elbe flood in August 2002. *Environ. Manage.* **38**: 717–732.

Raschendorfer M. 2001. The new turbulence parameterization of LM. *COSMO Newsletter* **1**: 89–97. http://www. cosmo-model.org.

Richard E, Cosma S, Benoit R, Binder P, Buzzi A, Kaufmann P. 2003a. Intercomparison of mesoscale meteorological models for precipitation forecasting. *Hydrol. Earth Sys. Sci.* **7**: 799–811.

Richard E, Cosma S, Tabary P, Pinty JP, Hagen M. 2003b. High-resolution numerical simulations of the convective system observed in the Lago Maggiore area on 17 September 1999 (MAP IOP2a). *Q. J. R. Meteorol. Soc* **129**: 543–563.

Richard E, Buzzi A, Zängl G. 2007. Quantitative precipitation forecasting in the Alps: The advances achieved by the Mesoscale Alpine Programme. *Q. J. R. Meteorol. Soc* **133**: 831–846.

Ritter B, Geleyn J. 1992. A comprehensive radiation scheme for numerical weather prediction models with potential applications in climate simulations. *Mon. Weather Rev.* **120**: 303–325.

Rudolf B, Frank H, Grieser J, Müller-Westermeier G, Rapp J, Trampf W. 2006. *Das Hochwasser in Südbayern im August 2005. Niederschlagsvorhersge, Warnung und klimatologische Bewertung des DWD*. DWD: Offenbach. http://www.hnd.bayern.de/ereignisse/hw220 805/links/Hochwasser-Bayern-2005.pdf.

Schär C, Durran DR. 1997. Vortex formation and vortex shedding in continuously stratified flows past isolated topography. *J. Atmos. Sci.* **54**: 534–554.

Schär C, Davies TD, Frei C, Wanner H, Widmann M, Wild M, Davies HC. 1998. Current Alpine Climate. Chapter 2 in: *Views from the Alps: Regional perspectives on climate change*. Cebon P, Dahinden U, Davies HC, Imboden DM, Jäger C. (eds), MIT Press: Boston, USA.

Schmidli J, Frei C. 2005. Trends of heavy precipitation and wet and dry spells in Switzerland during the 20th century. *Int. J. Climatol.* **25**: 753–771.

Skamarock W, Klemp J. 1992. The stability of time-split numerical methods for the hydrostatic and the non-hydrostatic elastic equations. *Mon. Weather Rev.* **120**: 2109–2127.

Smith RB. 1979. The influence of mountains on the atmosphere. *Adv. Geophys.* **21**: 87–230.

Smith RB, Gronas S. 1993. Stagnation points and bifurcation in 3-D mountain air-flow. *Tellus* **45A**: 28–43.

Steppeler J, Doms G, Schattler U, Bitzer H, Gassmann A, Damrath U, Gregoric G. 2003. Meso-gamma scale forecasts using the nonhydrostatic model LM. *Meteorol. Atmos. Phys.* **82**: 75–96.

SwissRe. 2006. Natural catastrophes and man-made disasters 2005: High earthquake casualties, new dimension in windstorm losses. *Sigma* **2**: 1–40. http://www.swissre.com.

Taylor KE. 2001. Summarizing multiple aspects of model performance in a single diagram. *J. Geophys. Res.* **106**: 7183–7192.

Tiedtke M. 1989. A comprehensive mass flux scheme for cumulus parameterization in large-scale models. *Mon. Weather Rev.* **117**: 1779–1800.

Van Bebber WJ. 1890. *Meteorologie*. Verlag von Ferdinand Enke: Stuttgart.

Verbunt M, Walser A, Gurtz J, Montani A, Schär C. 2007. Probabilistic flood forecasting with a limited-area ensemble prediction system. *J. Hydrometeorol.* **8**: 897–909.

Walser A, Lüthi D, Schär C. 2004. Predictability of precipitation in a cloud-resolving model. *Mon. Weather Rev.* **132**: 560–577.

Warner TT, Peterson RA, Treadon RE. 1997. A tutorial on lateral boundary conditions as a basic and potentially serious limitation to regional numerical weather prediction. *Bull. Am. Meteorol. Soc.* **78**: 2599–2617.

Yuan H, Mullen SL, Gao X, Sorooshian S, Du J, Juang HMH. 2005. Verification of probabilistic quantitative precipitation forecasts over the southwest United States during winter 2002/03 by the RSM ensemble system. *Mon. Weather Rev.* **78**: 279–294.

Zängl G. 2004a. Numerical simulations of the 12–13 August 2002 flooding event in eastern Germany. *Q. J. R. Meteorol. Soc.* **130**: 1921–1940.

Zängl G. 2004b. The sensitivity of simulated orographic precipitation to model components other than cloud microphysics. *Q. J. R. Meteorol. Soc.* **130**: 1857–1875.

Zängl G. 2007a. Interaction between dynamics and cloud microphysics in orographic precipitation enhancement: A high-resolution modeling study of two north-Alpine heavy precipitation events. *Mon. Weather Rev.* **135**: 2817–2840.

Zängl G. 2007b. To what extent does increased model resolution improve simulated precipitation fields? A case study of two north-Alpine heavy-rainfall events. *Meteorol. Zeitschrift* **16**: 571–580.

Zhang F, Snyder C, Rotunno R. 2003. Effects of moist convection on mesoscale predictability. *J. Atmos. Sci.* **60**: 1173–1185.

DOI: 10.1002/qj